INTERNATIONAL JOURNAL FOR NUMERICAL METHODS IN FLUIDS
*Int. J. Numer. Meth. Fluids* 2009; **61**:498–513
Published online 26 November 2008 in Wiley InterScience (www.interscience.wiley.com). DOI: 10.1002/fld.1964

# Topology optimization of microfluidic mixers

Casper Schousboe Andreasen*,†, Allan Roulund Gersborg and Ole Sigmund

*Department of Mechanical Engineering, Solid Mechanics, Nils Koppels Allé, Technical University of Denmark, 2800 Kgs. Lyngby, Denmark*

SUMMARY

This paper demonstrates the application of the topology optimization method as a general and systematic approach for microfluidic mixer design. The mixing process is modeled as convection dominated transport in low Reynolds number incompressible flow. The mixer performance is maximized by altering the layout of flow/non-flow regions subject to a constraint on the pressure drop between inlet and outlet. For a square cross-sectioned pipe the mixing is increased by 70% compared with a straight pipe at the cost of a 2.5 fold increase in pressure drop. Another example where only the bottom profile of the channel is a design domain results in intricate herring bone patterns that confirm findings from the literature. Copyright © 2008 John Wiley & Sons, Ltd.

Received 27 June 2008; Revised 6 October 2008; Accepted 6 October 2008

KEY WORDS: topology optimization; microfluidic mixing; stabilized FEM; convection dominated transport; sensitivity analysis; finite element methods; porous media; optimization; incompressible flow; Navier–Stokes; transport; micro-fluids; laminar flow

## 1. INTRODUCTION

Static microfluidic mixers appear in an abundance of different configurations, having all kinds of mixing improvers such as slanted grooves, herring bones, zig-zag walls, etc. The great variety of microfluidic mixers originate from the fact that the flow is laminar with a small Reynolds number. Therefore the mixing process relies mainly on the diffusive properties of the transported matter (see e.g. [1] for an introduction to mixing in microfluidics). To mix solutes with poor

*Correspondence to: Casper Schousboe Andreasen, Department of Mechanical Engineering, Solid Mechanics, Nils Koppels Allé, Technical University of Denmark, 2800 Kgs. Lyngby, Denmark.
†E-mail: csan@mek.dtu.dk

Contract/grant sponsor: DCAMM Research School through a grant from the Danish Agency for Science, Technology and Innovation
Contract/grant sponsor: Eurohorcs/ESF European Young Investigator Award (EURYI): 'Synthesis and topology optimization of optomechanical systems'
Contract/grant sponsor: Danish Center for Scientific Computing (DCSC)

diffusive properties, one can alter the geometry such that the flow distributes the matter more evenly in the solvent. By doing so, convection of matter is used as a mechanism to enhance mixing which; however, comes at the cost of an increased pressure drop between inlet and outlet. Stroock *et al*. [2] presented a mixer that induces chaotic advection by sequencing asymmetric microchannel sections containing staggered herringbones. For the systematic design of such microchannel mixers, topology optimization could be useful since no prerequisites are taken with respect to the geometry, only a design domain and boundary conditions need to be specified *a priori*.

The material distribution method for topology optimization was first presented by Bendsøe and Kikuchi [3] for solid mechanics problems. Since then, topology optimization has been introduced in several other branches of physics such as optics, acoustics and flows (see e.g. Bendsøe and Sigmund [4] for an overview of the subject).

Optimal design in fluid mechanics has been studied long before topology optimization was invented and optimal shapes minimizing the dissipated power for different profiles subjected to Stokes flow were already determined analytically in the 1970s by Pironneau [5] using shape optimization. As opposed to shape optimization, however, topology optimization allows introduction of new boundaries as the optimization progresses. This allows the topology to change several times during the optimization, which is impossible in shape optimization where the topology (i.e. the number of boundaries and connectivity) is predetermined.

In topology optimization the geometry is represented as a gray-scale image. The color in each pixel (finite element) represents a value of a physical parameter, e.g. permeability, such that black pixels represent small permeability (no-flow regions with 'solid-like' material) and white pixels represent large permeability (fluid regions). Computationally, the gray-scale in each element is a design variable. Based on repeated finite element analyses the design variables are updated using gradient driven math programming tools as described in e.g. [4].

Topology optimization in fluid mechanics was introduced by Borrvall and Petersson [6] modeling 2D flow in a Brinkman medium minimizing the dissipated power. The flow modeling was restricted to incompressible Stokes flow, neglecting the influence of inertia. In order to relax the optimization problem from an integer (black–white) problem where either fluid or solid property is allowed in an element, a porous flow model was introduced with a continuous (gray) permeability variable for each element. This leads to a design problem where flow and (all-most) non-flow regions develop by allowing interpolation between the lower and upper value of the permeability. The mathematical foundation was further investigated by Evgrafov [7] and the limiting cases of pure fluid and solid were included. A variation of the approach is presented in Guest and Prévost [8] where the Stokes and Darcy equations exist as two different models that are combined and scaled according to the permeability of each element. Furthermore, stabilized finite elements were used in order to use equal order velocity and pressure interpolation, as well as for avoiding a singular perturbation problem due to the coupled Stokes–Darcy problem. Wiker *et al*. [9] also considered topology optimization of Darcy–Stokes problems with focus on area-to-point flow problems.

The method has been extended to cover low to moderate Reynolds number flows in 2D, though still in the laminar regime, by Gersborg-Hansen *et al*. [10] and Olesen *et al*. [11]. The well posedness of the extension to the incompressible Navier–Stokes equations was discussed in detail by Evgrafov [12]. With respect to topology optimization of fluid transport problems, Thellner [13] provided examples with heat-transfer in 2D Stokes flow, Gersborg-Hansen [14] considered a convection dominated transport problem in a 2D rectangular microchannel and Okkels and Bruus [15] have investigated 2D catalytic microfluidic reactors. Recently, other approaches such as the



DOI: 10.1002/fld

lattice Boltzmann method by Pingen *et al*. [16] and kinetic gas theory by Evgrafov *et al*. [17] have been presented as alternative simulation methods.

Little work has been presented using 3D simulation methods, mainly due to the many design iterations, which limit the problem sizes in order to achieve an acceptable execution time. Recently, Pingen *et al*. [16] showed 3D nozzle design and Aage *et al*. [18] presented 3D Stokes flow problems and minimized the dissipative energy of some academic 3D problems which can be compared with the analytical results by Pironneau [5]. Three-dimensional Darcy–Stokes flow was also considered by Guest and Prévost [19] in order to optimize the permeability of material microstructures by a homogenization approach. Othmer [20] presents a method for implementing topology optimization of ducted flows with commercial CFD codes.

This work extends topology optimization of convection dominated transport problems to 3D. In this context, a standard streamline-upwind/Petrov–Galerkin (SUPG) stabilization scheme by Brooks and Hughes [21] is applied to stabilize the transport problem and the underlying flow problem is stabilized by the classical Galerkin-least-square (GLS) scheme by Hughes and Franca [22]. The former stabilization technique avoids numerical instabilities in transport problems due to a small coefficient of diffusion. The latter stabilization circumvents the Ladyzhenskaya–Babuška–Brezzi (LBB) condition, such that equal order velocity and pressure elements can be used to reduce the computational cost. The LBB condition is a compatibility condition that ensures convergence for the finite element problem, which in practice means that the polynomial order of the velocity interpolation should be one degree higher than the pressure interpolation.

The paper is organized as follows: Section 2 describes the continuous problem, Section 3 presents the stabilized finite element formulation, Section 4 introduces the topology optimization problem and associated sensitivity analysis and Section 5 covers further implementation aspects. Section 6 presents design examples and Section 7 contains a discussion and conclusions.

## 2. GOVERNING EQUATIONS

The flows considered in this paper are assumed to be microscale and therefore laminar. Furthermore, the flow speed is small compared with the speed of sound, which motivates a negligible compressibility; therefore the flow is modeled as incompressible. A porosity field is introduced in order to control the fluid paths through the domain. Regions with very high permeability can be considered pure fluid, whereas nearly no fluid can penetrate porous regions with low permeability. These low permeability regions are interpreted as solid regions.

For a domain $\Omega$ with partitioned boundary $\Gamma=\overline{\Gamma_{\text{in}}\cup\Gamma_{\text{wall}}\cup\Gamma_{\text{out}}}$, $\emptyset=\Gamma_{\text{in}}\cap\Gamma_{\text{wall}}\cap\Gamma_{\text{out}}$ cf. Figure 1, the porosity field is introduced in the steady-state Navier–Stokes equation as a source term $\alpha(\xi)\mathbf{u}$ yielding a Brinkman model with a convection term:

$$-\nabla\cdot(\mu(\nabla\mathbf{u}+(\nabla\mathbf{u})^{\mathrm{T}})-\mathbf{I}p)+\mathbf{u}\cdot\rho\nabla\mathbf{u}+\alpha(\xi)\mathbf{u}=\mathbf{0}\quad\text{in }\Omega \tag{1}$$

where $\alpha$ is the porosity field, $\xi$ is the spatially varying design variable field, $\mathbf{u}$ is the velocity field, $p$ is the pressure and $\mathbf{I}$ the identity tensor. The $\xi$ field is fixed in the flow problem and determined by the optimization algorithm described in Section 4. $\mu$ is the viscosity and $\rho$ is the mass density which are both constant throughout the domain. In this work the low Reynolds number limit is considered $Re=\rho U d_{\text{h}}/\mu<1$, where $U$ is a reference velocity (here mean velocity) and $d_{\text{h}}$ a length scale (here the hydraulic diameter). The hydraulic diameter is given by $d_{\text{h}}=4\mathscr{A}/\mathscr{O}$, where $\mathscr{A}$ is a cross-sectional area and $\mathscr{O}$ its circumference. The hydraulic diameter is a unification of the



DOI: 10.1002/fld

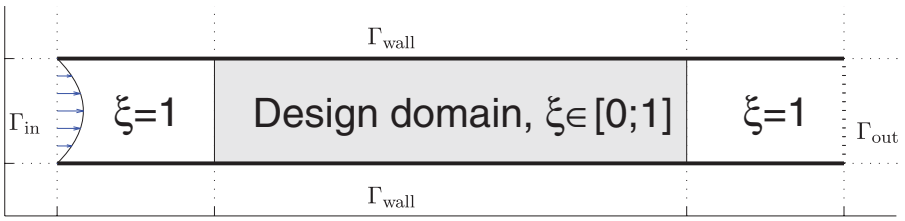


Figure 1. Principle sketch of the domain $\Omega$. The design variable field $\xi$ interpolates between a laminar flow model ($\xi=1$) and a model for porous flow ($\xi=0$). The boundary $\Gamma$ consists of an inlet, a wall and an outlet part.

characteristic length for pipes with arbitrary cross-section, such that flow conditions for e.g. square and circular cross-sectioned pipes can be compared. In order to perform topology optimization, the $\alpha$ term in an element may take a finite value in the interval $0 \leqslant \alpha < +\infty$.

The incompressibility imposed on the conservation of mass yields the continuity equation:

$$-\nabla \cdot \mathbf{u} = 0 \quad \text{in } \Omega \tag{2}$$

Transport of matter with the flow is modeled by a convection–diffusion equation:

$$\mathbf{u} \cdot \nabla \phi - \frac{1}{Pe} \nabla^2 \phi = 0 \quad \text{in } \Omega \tag{3}$$

where $\phi$ measures the concentration of the matter, $Pe = U d_{\text{h}} / D$ is the Péclet number with $U$ being a reference velocity (here mean velocity), $D$ is the diffusivity and $d_{\text{h}}$ the hydraulic diameter. In order to consider convection dominated transport, the $Pe \gg 1$ limit is considered and furthermore $Pe$ is constant throughout the domain. Finally, a one-way coupling is assumed such that the flow Equations (1)–(2) are independent of the concentration $\phi$ governed by Equation (3).

The boundary conditions for the mixing problem take the following form: At $\Gamma_{\text{in}}$ the velocity profile and a Heaviside concentration profile are prescribed (Dirichlet boundary conditions), at $\Gamma_{\text{wall}}$ the velocity and the concentration flux are zero (Dirichlet and Neumann boundary conditions, respectively) and $\Gamma_{\text{out}}$ is a free boundary where the pressure and normal stress are prescribed to zero and the concentration flux is zero (Neumann boundary conditions). In mathematical terms this becomes

$$\mathbf{u} = \mathbf{u}^*(s_1, s_2) \quad \text{and} \quad \phi(s_1) = \begin{cases} 0, & s_1 < 0.5 \\ 1, & s_1 = 0.5 \\ 2 & \text{otherwise} \end{cases} \quad \text{on } \Gamma_{\text{in}} \tag{4}$$

$$\mathbf{u} = \mathbf{0} \quad \text{and} \quad \nabla \phi \cdot \mathbf{n} = 0 \quad \text{on } \Gamma_{\text{wall}} \tag{5}$$

$$p = 0, \ (\mu(\nabla \mathbf{u} + (\nabla \mathbf{u})^{\text{T}}) - p\mathbf{I}) \cdot \mathbf{n} = \mathbf{0} \quad \text{and} \quad \nabla \phi \cdot \mathbf{n} = 0 \quad \text{on } \Gamma_{\text{out}} \tag{6}$$

where $\mathbf{I}$ is the identity tensor, $\mathbf{n}$ is the outward unit normal vector and $(s_1, s_2)$ parameterize the boundaries $\Gamma_{\text{in}}$ and $\Gamma_{\text{out}}$ with $(s_1, s_2) \in [0; 1]^2$.



DOI: 10.1002/fld

## 3. FINITE ELEMENT FORMULATION

The finite element trial and test function spaces $\mathscr{J}_{\mathbf{u}}^{\mathrm{h}}$ and $\mathscr{V}_{\mathbf{u}}^{\mathrm{h}}$ for velocity, $\mathscr{J}_{p}^{\mathrm{h}}=\mathscr{V}_{p}^{\mathrm{h}}$ for pressure and $\mathscr{J}_{\phi}^{\mathrm{h}}$, $\mathscr{V}_{\phi}^{\mathrm{h}}$ for concentration are defined on $\Omega$ by use of tri-linear polynomials. For the design variable field $\xi$, the finite element trial and test function spaces $\mathscr{J}_{\xi}^{\mathrm{h}}=\mathscr{V}_{\xi}^{\mathrm{h}}$ are defined on $\Omega$ by use of piecewise constant polynomials. For the flow problem, this equal order interpolation of the velocity and the pressure fields does not fulfill the LBB condition [23], which is revealed numerically by pressure oscillations, if none or insufficient stabilization is introduced. The standard procedure to circumvent this is to use a GLS stabilized weak form [22], which penalizes large pressure gradients. With GLS stabilization the weak form of the flow Equations (1)–(2) is given as

Find $\mathbf{u}^{\mathrm{h}}\in\mathscr{J}_{\mathbf{u}}^{\mathrm{h}}$ and $p^{\mathrm{h}}\in\mathscr{J}_{p}^{\mathrm{h}}$ such that $\forall\hat{\mathbf{u}}^{\mathrm{h}}\in\mathscr{V}_{\mathbf{u}}^{\mathrm{h}}$ and $\forall\hat{p}^{\mathrm{h}}\in\mathscr{V}_{p}^{\mathrm{h}}$

$$\begin{aligned}&\mu\int_{\Omega}\nabla\hat{\mathbf{u}}^{\mathrm{h}}\cdot(\nabla\mathbf{u}^{\mathrm{h}}+(\nabla\mathbf{u}^{\mathrm{h}})^{\mathrm{T}})\,\mathrm{d}\Omega+\int_{\Omega}\hat{\mathbf{u}}^{\mathrm{h}}\cdot(\mathbf{u}^{\mathrm{h}}\cdot\rho\nabla\mathbf{u}^{\mathrm{h}})\,\mathrm{d}\Omega+\int_{\Omega}\hat{\mathbf{u}}^{\mathrm{h}}\cdot\alpha\mathbf{u}^{\mathrm{h}}\,\mathrm{d}\Omega\\&-\int_{\Gamma_{\mathrm{out}}}\hat{\mathbf{u}}^{\mathrm{h}}\cdot(\mu(\nabla\mathbf{u}^{\mathrm{h}}+(\nabla\mathbf{u}^{\mathrm{h}})^{\mathrm{T}})-\mathbf{I}p^{\mathrm{h}})\cdot\mathbf{n}\,\mathrm{d}\Gamma-\int_{\Omega}p^{\mathrm{h}}(\nabla\cdot\hat{\mathbf{u}}^{\mathrm{h}})\,\mathrm{d}\Omega-\int_{\Omega}\hat{p}^{\mathrm{h}}(\nabla\cdot\mathbf{u}^{\mathrm{h}})\,\mathrm{d}\Omega\\&+\sum_{e=1}^{n_{\mathrm{el}}}\int_{\Omega^{e}}\tau_{\mathrm{GLS}}(\nabla\hat{p}^{\mathrm{h}}\cdot\nabla p^{\mathrm{h}})\,\mathrm{d}\Omega=\mathbf{0}\end{aligned}\tag{7}$$

where $n_{\mathrm{el}}$ is the number of elements and $\Omega^{e}$ the domain for element $e$. The boundary term is zero since $\Gamma_{\mathrm{out}}$ is a free boundary cf. Equation (6). Here the stabilization parameter is chosen as

$$\tau_{\mathrm{GLS}}=\alpha_{0}\frac{\rho h_{e}^{2}}{4\mu}\tag{8}$$

where $h_e$ is the element size and $\alpha_0=\frac{1}{3}$ as this appears to be the optimal value for linear elements [24]. Moreover, for the Stokes problem ($\rho=0,\alpha=0$) with linear velocity interpolation, this stabilization scheme is consistent since it yields a zero residual for an exact solution to the Stokes equations. The GLS stabilization deals with the LBB condition, but it does not fix the problems arising due to high flow speeds [24, 25]. In addition, in the very low permeability (Darcy) limit, stabilization may be required [26] also in the context of topology optimization [8]. However, since our scope is the transport in low speed laminar flow rather than high speed flows or transport in Darcy flows, both these stabilization techniques have been left out of this study.

In order to model convection dominated transport the transport problem is also stabilized to avoid using an extremely fine mesh resulting in large computation times. The weak form of Equation (3) including SUPG stabilization [21] yields

Find $\phi^{\mathrm{h}}\in\mathscr{J}_{\phi}^{\mathrm{h}}$ such that $\forall\hat{\phi}^{\mathrm{h}}\in\mathscr{V}_{\phi}^{\mathrm{h}}$:

$$\begin{aligned}&\int_{\Omega}\hat{\phi}^{\mathrm{h}}(\mathbf{u}^{\mathrm{h}}\cdot\nabla\phi^{\mathrm{h}})\,\mathrm{d}\Omega+\frac{1}{Pe}\int_{\Omega}\nabla\hat{\phi}^{\mathrm{h}}\cdot\nabla\phi^{\mathrm{h}}\,\mathrm{d}\Omega-\frac{1}{Pe}\int_{\Gamma_{\mathrm{wall}}\cup\Gamma_{\mathrm{out}}}\hat{\phi}^{\mathrm{h}}\nabla\phi^{\mathrm{h}}\cdot\mathbf{n}\,\mathrm{d}\Gamma\\&+\sum_{e=1}^{n_{\mathrm{el}}}\int_{\Omega^{e}}\tau_{\mathrm{SUPG}}\mathbf{u}^{\mathrm{h}}\cdot\nabla\hat{\phi}^{\mathrm{h}}\underbrace{\left(\mathbf{u}^{\mathrm{h}}\cdot\nabla\phi^{\mathrm{h}}-\nabla\cdot\left(\frac{1}{Pe}\nabla\phi^{\mathrm{h}}\right)\right)}_{\text{Strong form residual}}\mathrm{d}\Omega=0\end{aligned}\tag{9}$$



DOI: 10.1002/fld

where the boundary term is zero due to the boundary conditions imposed on $\phi$. Notice, that for linear elements the second contribution in the residual is zero, thus large concentration gradients in the streamwise direction are penalized. Here the stabilization parameter $\tau_{\mathrm{SUPG}}$ is determined as described in [27]

$$\tau_{\mathrm{SUPG}} = \left( \frac{4}{h_e^2 Pe} + \frac{2|\mathbf{u}^{\mathrm{h}}|}{h_e} \right)^{-1} \tag{10}$$

## 4. TOPOLOGY OPTIMIZATION

The optimization problems considered are mixing problems with the aim of determining the optimal material layout. The procedure is that a given spatial domain is divided into small (finite) elements where each of these can be either solid(black) or fluid(white). This yields an integer problem, which is difficult to solve computationally due to its non-differentiable nature. In order to deal with this, the optimization problem is relaxed by introducing continuous design variables, which can take any value between 0 (no flow) and 1 (fluid). The design variables enter the flow equation through the inverse permeability function $\alpha(\xi)$, cf. Equation (1). The optimization problem can then be stated as

$$\begin{aligned}
\min_{\boldsymbol{\xi}} \quad & \Phi = \frac{1}{\langle\phi\rangle_{\mathrm{in}}^2 \int_{\Gamma_{\mathrm{in}}} 1 \,\mathrm{d}\Gamma} \int_{\Gamma_{\mathrm{out}}} (\phi^{\mathrm{h}} - \langle\phi\rangle_{\mathrm{in}})^2 \,\mathrm{d}\Gamma \\
\text{s.t.} \quad & \text{Governing equations (7), (9)} \\
& \Delta p \leqslant \beta \Delta p_{\mathrm{ref}} \\
& \alpha_e(\xi_e) = \overline{\alpha} + (\underline{\alpha} - \overline{\alpha}) \xi_e \frac{1+q}{\xi_e + q} \quad \text{for } e = 1, \ldots, n_{\mathrm{el}} \\
& 0 \leqslant \xi_e \leqslant 1 \quad \text{for } e = 1, \ldots, n_{\mathrm{el}}
\end{aligned} \tag{11}$$

where $\boldsymbol{\xi} \in \mathbb{R}^{n_{\mathrm{el}}}$ is a vector of element design variables, which parameterizes the design variable field $\xi^{\mathrm{h}}$, $n_{\mathrm{el}}$ is the number of elements and $\Phi$ is the cost function, which measures the mixing performance. The mixing performance is defined as the difference between the concentration at the outlet and the average inlet concentration $\langle\phi\rangle_{\mathrm{in}} = \int_{\Gamma_{\mathrm{in}}} \phi^{\mathrm{h}} \,\mathrm{d}\Gamma / \int_{\Gamma_{\mathrm{in}}} 1 \,\mathrm{d}\Gamma$ normalized with respect to the average inlet concentration, such that an ideal mixer will have the performance $\Phi_{\mathrm{ideal}} = 0$ due to conservation of mass, see Figure 2. The governing equations enter as constraints in the optimization problem and in order to control the pressure drop $\Delta p = \int_{\Gamma_{\mathrm{in}}} p^{\mathrm{h}} \,\mathrm{d}\Gamma$ between the inlet and the outlet, another constraint is imposed which limits it to a factor $\beta$ times the pressure drop of the initial and empty straight pipe corresponding to $\boldsymbol{\xi} = \mathbf{1}$. The absolute pressure is fixed at zero at the outlet and therefore it does not enter into the constraint. The interpolation function $\alpha$ was first introduced by Borrvall and Petersson [6] and it plays an important role in topology optimization. The optimal material distribution for Stokes flow problems in terms of minimum pressure drop is black–white, i.e. as opposed to the interpolation used in e.g. topology optimization of solid structures [4], intermediate values of $\xi$ (gray elements) are not favorable. Thus the minimum pressure drop problem in Stokes flow is self-penalized and the $\alpha$ function ensures that gray elements can appear in the problem. Gray elements are important in order to prohibit an integer nature of the optimization problem during the early design process. Moreover, from a physical point of



DOI: 10.1002/fld

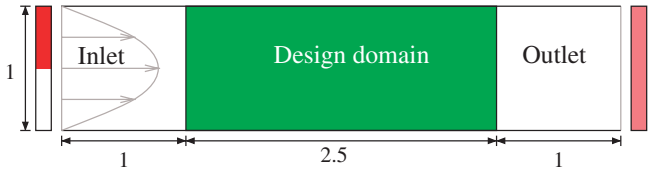


Figure 2. General problem definition for mixing problems. The modeling domain is divided into three subdomains: inlet, outlet and design domain. Flow field: The inlet velocity profile is parabolic in order to model fully developed pipe flow. The horizontal walls have a no slip condition $\mathbf{u}=0$ and the outlet is free such that normal stress $(\mu(\nabla\mathbf{u}+(\nabla\mathbf{u})^{\mathrm{T}})-p\mathbf{I})\cdot\mathbf{n}=\mathbf{0}$ and $p=0$. The concentration field: Heaviside profile at the inlet, no flux conditions at the horizontal walls $\nabla\phi\cdot\mathbf{n}=0$ and free at the outlet where the performance of the mixer is computed. The concentration is illustrated by the Heaviside function illustrated at the inlet and a uniform distribution at the outlet.

view the term $\alpha\mathbf{u}$, cf. Equation (1), penalizes large velocities in regions with low permeability. Even though the mixing problem is not a minimum pressure drop problem, the same interpolation function is used as it appears to work well, which we attribute to the pressure drop constraint. The bound values on $(\underline{\alpha},\overline{\alpha})=(0,10^4)$, are the minimum and maximum inverse permeabilities, $q$ is a penalization parameter, here $q=1$. The zero lower bound on the inverse permeability is motivated from a physical point of view since the free stream is governed by the Navier–Stokes equations and the well posedness of the optimization problem for $\underline{\alpha}=0$ was considered in [7]. The last line in (11) defines box constraints on the design variables.

The optimization problem is solved using the method of moving asymptotes (MMA) [28], which works well for optimization problems with many design variables but few constraints. It is a gradient-based optimization algorithm that solves several convex and separable subproblems by an interior point method for each design iteration. In order to use the pressure drop constraint with the MMA algorithm it is turned into a function yielding a negative value if feasible and positive if violated. The pressure drop constraint is expressed as

$$g=\frac{\Delta p}{\beta\Delta p_{\mathrm{ref}}}-1\leqslant 0 \tag{12}$$

In the field of topology optimization a volume constraint is often imposed. However, for mixer design problems a volume constraint, limiting the amount of solid material, is hardly relevant since material weight is not an issue. Instead we impose the pressure drop constraint, which has obvious physical relevance.

### *4.1. Adjoint sensitivity analysis*

In order to achieve consistent sensitivities the adjoint sensitivity analysis method [20, 29–31] is utilized resulting in new linear partial differential equations (PDEs) that need to be solved in order to compute the sensitivities. This is done by forming the Lagrangian, the sum of the objective function and the weak expressions for the state Equations (7)–(9) evaluated with the state solution $(\mathbf{u}^{\mathrm{h}},p^{\mathrm{h}},\phi^{\mathrm{h}})$ and with Lagrange multiplier fields $(\boldsymbol{\lambda}_{\mathbf{u}}^{\mathrm{h}},\lambda_p^{\mathrm{h}},\lambda_\phi^{\mathrm{h}})$ instead of the test functions $(\hat{\mathbf{u}}^{\mathrm{h}},\hat{p}^{\mathrm{h}},\hat{\phi}^{\mathrm{h}})$, and differentiating it with respect to the design variables. By rearranging the resulting expression, adjoint problems arise which when solved eliminate the direct computations of $\mathrm{d}\mathbf{u}^{\mathrm{h}}/\mathrm{d}\boldsymbol{\xi}$, $\mathrm{d}p^{\mathrm{h}}/\mathrm{d}\boldsymbol{\xi}$ and $\mathrm{d}\phi^{\mathrm{h}}/\mathrm{d}\boldsymbol{\xi}$, which are computationally expensive due to the large number of design



DOI: 10.1002/fld

variables. The result is an adjoint transport problem, where $\lambda_\phi^{\mathrm{h}}$ is the adjoint concentration field:

Find $\lambda_\phi^{\mathrm{h}} \in \mathscr{J}_\phi^{\mathrm{h}}$ such that $\forall \hat{\lambda}_\phi^{\mathrm{h}} \in \mathscr{V}_\phi^{\mathrm{h}}$

$$\int_\Omega \left( \lambda_\phi^{\mathrm{h}} (\mathbf{u}^{\mathrm{h}} \cdot \nabla \hat{\lambda}_\phi^{\mathrm{h}}) + \frac{1}{Pe} \nabla \lambda_\phi^{\mathrm{h}} \cdot \nabla \hat{\lambda}_\phi^{\mathrm{h}} \right) \mathrm{d}\Omega + \int_\Omega (\mathbf{u}^{\mathrm{h}} \cdot \nabla \lambda_\phi^{\mathrm{h}}) \tau_{\mathrm{SUPG}} \left( \mathbf{u}^{\mathrm{h}} \cdot \nabla \hat{\lambda}_\phi^{\mathrm{h}} - \frac{1}{Pe} \nabla^2 \hat{\lambda}_\phi^{\mathrm{h}} \right) \mathrm{d}\Omega$$
$$+ \frac{2}{\langle \phi \rangle_{\mathrm{in}}^2 \int_{\Gamma \mathrm{in}} 1 \, \mathrm{d}\Gamma} \int_{\Gamma_{\mathrm{out}}} \hat{\lambda}_\phi^{\mathrm{h}} (\phi - \langle \phi \rangle_{\mathrm{in}}) \, \mathrm{d}\Gamma = 0 \tag{13}$$

Having solved the adjoint transport problem, the adjoint flow problem (with unknowns $\boldsymbol{\lambda}_{\mathbf{u}}^{\mathrm{h}}$ and $\lambda_p^{\mathrm{h}}$) can be solved where the adjoint concentration appears on the right-hand side:

Find $\boldsymbol{\lambda}_{\mathbf{u}}^{\mathrm{h}} \in \mathscr{J}_{\mathbf{u}}^{\mathrm{h}}$ and $\lambda_p^{\mathrm{h}} \in \mathscr{J}_p^{\mathrm{h}}$ such that $\forall \hat{\boldsymbol{\lambda}}_{\mathbf{u}}^{\mathrm{h}} \in \mathscr{V}_{\mathbf{u}}^{\mathrm{h}}$ and $\forall \hat{\lambda}_p^{\mathrm{h}} \in \mathscr{V}_p^{\mathrm{h}}$:

$$\int_\Omega [\nabla \boldsymbol{\lambda}_{\mathbf{u}}^{\mathrm{h}} \cdot \mu (\nabla \hat{\boldsymbol{\lambda}}_{\mathbf{u}}^{\mathrm{h}} + (\nabla \hat{\boldsymbol{\lambda}}_{\mathbf{u}}^{\mathrm{h}})^{\mathrm{T}}) - \lambda_p^{\mathrm{h}} (\nabla \cdot \hat{\boldsymbol{\lambda}}_{\mathbf{u}}^{\mathrm{h}}) + \boldsymbol{\lambda}_{\mathbf{u}}^{\mathrm{h}} \cdot (\hat{\boldsymbol{\lambda}}_{\mathbf{u}}^{\mathrm{h}} \cdot \rho \nabla \mathbf{u}^{\mathrm{h}} + \mathbf{u}^{\mathrm{h}} \cdot \rho \nabla \hat{\boldsymbol{\lambda}}_{\mathbf{u}}^{\mathrm{h}})$$
$$+ \boldsymbol{\lambda}_{\mathbf{u}}^{\mathrm{h}} \cdot \alpha(\xi) \hat{\boldsymbol{\lambda}}_{\mathbf{u}}^{\mathrm{h}}] \, \mathrm{d}\Omega - \int_\Omega \hat{\lambda}_p^{\mathrm{h}} (\nabla \cdot \boldsymbol{\lambda}_{\mathbf{u}}^{\mathrm{h}}) \, \mathrm{d}\Omega + \sum_{e=1}^{n_{\mathrm{el}}} \int_{\Omega^e} \tau_{\mathrm{GLS}} (\nabla \lambda_p^{\mathrm{h}} \cdot \nabla \hat{\lambda}_p^{\mathrm{h}}) \, \mathrm{d}\Omega$$
$$= - \int_\Omega \lambda_\phi^{\mathrm{h}} (\hat{\boldsymbol{\lambda}}_{\mathbf{u}}^{\mathrm{h}} \cdot \nabla \phi^{\mathrm{h}}) \, \mathrm{d}\Omega - \int_\Omega \left( \frac{\partial \tau_{\mathrm{SUPG}}}{\partial \mathbf{u}^{\mathrm{h}}} \cdot \hat{\boldsymbol{\lambda}}_{\mathbf{u}}^{\mathrm{h}} \right) \mathbf{u}^{\mathrm{h}} \cdot \nabla \lambda_\phi^{\mathrm{h}} \left( \mathbf{u}^{\mathrm{h}} \cdot \nabla \phi^{\mathrm{h}} - \frac{1}{Pe} \nabla^2 \phi^{\mathrm{h}} \right) \mathrm{d}\Omega$$
$$- \int_\Omega \tau_{\mathrm{SUPG}} \left[ \hat{\boldsymbol{\lambda}}_{\mathbf{u}}^{\mathrm{h}} \cdot \nabla \lambda_\phi^{\mathrm{h}} \left( \mathbf{u}^{\mathrm{h}} \cdot \nabla \phi^{\mathrm{h}} - \frac{1}{Pe} \nabla^2 \phi^{\mathrm{h}} \right) + \mathbf{u}^{\mathrm{h}} \cdot \nabla \lambda_\phi^{\mathrm{h}} (\hat{\boldsymbol{\lambda}}_{\mathbf{u}}^{\mathrm{h}} \cdot \nabla \phi^{\mathrm{h}}) \right] \mathrm{d}\Omega \tag{14}$$

where

$$\frac{\partial \tau_{\mathrm{SUPG}}}{\partial \mathbf{u}^{\mathrm{h}}} = - \frac{2 \mathbf{u}^{\mathrm{h}}}{h_e |\mathbf{u}^{\mathrm{h}}|} \left( \frac{4}{{h_e}^2 Pe} + \frac{2 |\mathbf{u}^{\mathrm{h}}|}{h_e} \right)^{-2} \tag{15}$$

Inserting the adjoint solutions in the expression for the sensitivities of the Lagrangian results in the following simple expression:

$$\frac{\mathrm{d}\Phi}{\mathrm{d}\boldsymbol{\xi}} = \int_\Omega \hat{\xi}^{\mathrm{h}} \boldsymbol{\lambda}_{\mathbf{u}}^{\mathrm{h}} \cdot \frac{\partial \alpha}{\partial \xi} \mathbf{u}^{\mathrm{h}} \, \mathrm{d}\Omega \tag{16}$$

where $\hat{\xi}^{\mathrm{h}}$ is the test function (shape function) for the design variable field $\xi^{\mathrm{h}}$. It should be noted though, that the introduction of this test function is only a very convenient way to introduce the design variable field and thereby sensitivities in COMSOL and the variable is newer being solved for cf. [11].

Finally, the sensitivity of the constraint function $g$ needs to be computed. This can be done analogously, but with the difference that no adjoint transport problem appears for this case since the pressure only appears in the flow equations. The right-hand side of Equation (14) then becomes

$$\mathrm{RHS} = \frac{-1}{\beta \Delta p_{\mathrm{ref}}} \int_{\Gamma_{\mathrm{in}}} \hat{\lambda}_p^{\mathrm{h}} \, \mathrm{d}\Gamma \tag{17}$$

where $\beta$ and $\Delta p_{\mathrm{ref}}$ are fixed constants cf. Equation (11).

### *4.2. Density filter*

It is common to use regularization techniques to ensure well-posed topology optimization problems [32]. The density filter approach used in this work was introduced by Bruns and Tortorelli [33],



DOI: 10.1002/fld

its convergence was proven by Bourdin [34] and it has recently been reviewed and extended by Sigmund [35]. The density filter has some attractive properties. Apart from removing mesh dependency by ensuring a minimum length scale in the optimized topology, it also tends to convexify the optimization problem leading to better convergence. Contrary to creeping flow problems where mesh dependency is not an issue cf. [6], the optimized topologies for mixing problems seem to exhibit some mesh dependency when the Péclet and Reynolds numbers are increased.

For the second example problem, presented later, the filter has been imposed from the beginning. After convergence it has been turned off and the optimization has been continued in order to increase the contrast in the permeability.

## 5. IMPLEMENTATION

For the implementation of the finite element method COMSOL Multiphysics 3.4, a high level PDE toolbox that can be integrated with Matlab, is utilized. The package includes routines for all parts of the analysis; meshing, assembling, solving and plotting. This leaves the main focus on the formulation of the objective function, formulation of interpolation functions, implementation of the sensitivity analysis and the communication with the optimization algorithm. The adjoint sensitivity analysis is performed on the same mesh as the original problem, and the sensitivities, Equation (16), are obtained by formulating an artificial problem and retrieving the right-hand side using the assembly procedure in a manner similar to Olesen *et al*. [11]. Moreover, a correct implementation of the sensitivity calculation was confirmed by a finite difference check. To solve the optimization problem the MMA [28] is used.

The initial conditions for the design field is a random uniform distribution, such that unsymmetries in the final design can be triggered if they are desired, which might be a problem if the initial distribution is uniform. The high level programming language approach makes it possible to implement and test different methods and approaches easily on academic size problems. The following flowchart presents the optimization procedure:

1. Initialization
   *Set up equation system*, *compute reference values*, *filter-neighborhood*, *initialize iteration counter* $i=1$, *etc*.
2. Apply filter to design variables
3. Solve the state problems by FEM, Equations (7), (9)
4. Compute the objective and constraint value, Equations (11), (12)
5. Compute sensitivities $(\Phi', g')$ by the adjoint method, Equations (13)–(14), (16)–(17)
6. Apply filter to sensitivities (chain rule)
7. Update design variables $\xi$ by MMA call
8. Check for convergence $\|\xi^i - \xi^{i-1}\|_\infty \ll 1\%$
   *If convergence is not reached*, *go to 2 and increase iteration counter* $i=i+1$
   *else continue*
9. Post processing



DOI: 10.1002/fld

As it is seen from the flowchart, the state and adjoint problems will be solved several times, therefore some effort has been invested in representing and solving the equation system as efficiently as possible. This is the reason for choosing a first-order velocity–pressure pair and to compensate by stabilizing the formulation instead of using the LBB stable Taylor–Hood pair (second-order velocity, first-order pressure). In order to solve the equation systems, the *Pardiso* solver implemented in COMSOL is used, as it is a fast direct solver that to some extent is able to make use of multiple processors. An iterative solver (*GMRES*) has also been tested and performs well, though it cannot outperform the direct solver for the problem sizes used in this paper.

The computational environment used was a double dual-core Intel Xeon 5160 3.00 GHz with 16 GB RAM running GNU/Linux 2.6.9-55.ELsmp, COMSOL 3.4 and Matlab 7.4 (R2007a). With this configuration the total execution time was approximately 92 and 136 h for the two micromixer examples, having approx. 160.000 and 340.000 state dofs in each of the flow problems, respectively.

## 6. DESIGN EXAMPLES

### *6.1. Micromixer with prescribed pressure drop*

As a first test case a channel with square cross-section as seen in Figure 3 is considered. Only the middle section of the channel is included as a design domain in order to avoid boundary effects influencing on the optimized design. The design variables are initially given random values and as the optimization progresses the material is redistributed and an optimized topology is achieved which is shown in Figure 4, and a plot of the concentration along the channel is shown in Figure 5. The performance of the optimized mixer is $\Phi_{\text{opt}} = 0.2051$ compared with the $\Phi_{\text{empty}} = 0.6786$ of the empty pipe, which is an improvement of 70% at the cost of a 2.5 fold increase in the pressure drop compared with the empty straight pipe (enforced via the pressure drop constraint with $\beta = 2.5$). It is seen that even though there is a great improvement in the mixing, the solute still has regions of high and low concentrations. By allowing a larger pressure drop the mixing can be further improved (see below). The stretching and folding that occurs in the mixer is visualized in Figure 5. It is interesting to note that the optimized topology does not have any unattached solid elements

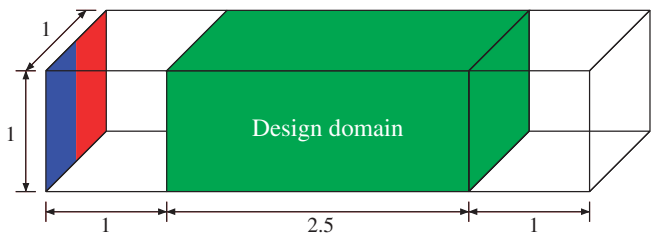


Figure 3. Pipe with square cross-section having outer measures $1 \times 1 \times 4.5$ and a design domain of length 2.5 in order to avoid influence from boundary conditions on the design. Parabolic inflow profile to the left with a Heaviside concentration distribution. No slip at horizontal faces and free outlet at the right vertical face.



DOI: 10.1002/fld

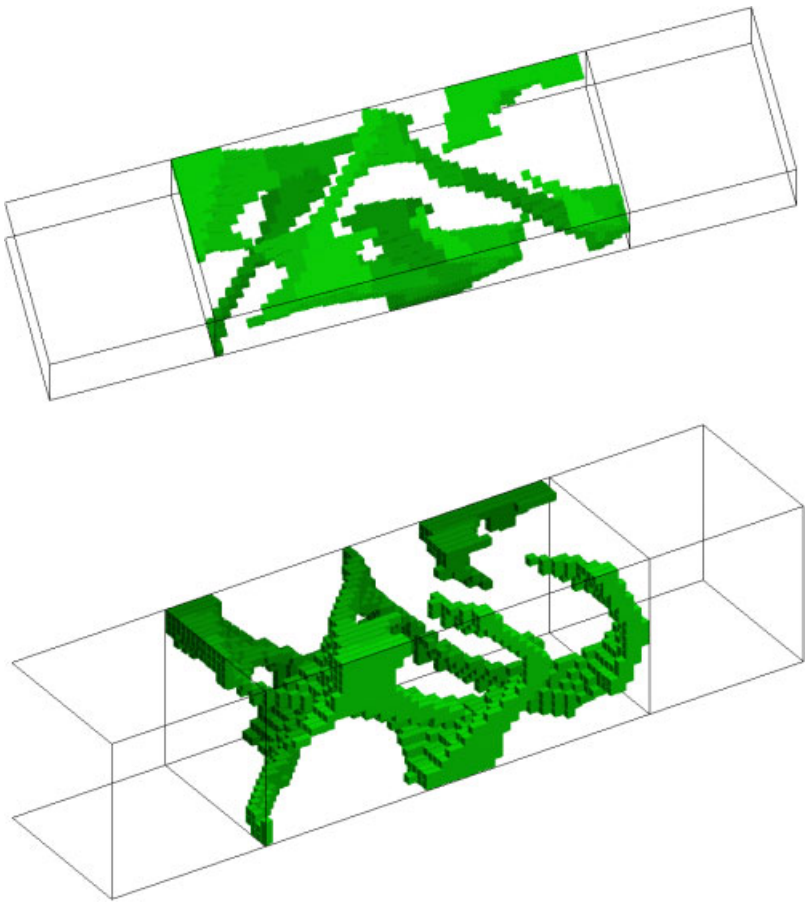

Figure 4. Optimized topology for Stokes flow ($\rho=0, \mu=1$) with $Pe=1000$ in the square cross-sectioned pipe. Design variables plotted with threshold $\xi<0.5$, colored by depth. Design variable distribution: $\xi<0.1:10\%$, $\xi>0.9:89\%$. Problem details: 20 000 ($20\times20\times50$) design variables. Final objective $\Phi_{\text{final}}=0.2051$, reference objective $\Phi_{\text{empty}}=0.6786$. Allowed pressure drop $\beta=2.5$. Computation time approx. 92 h. Iterations: 1041 without filter.

even though this was not implemented as a constraint. Most probably isolated solid regions would cause too much pressure loss compared with their mixing performance.

In order to study the influence of the allowed pressure drop $\beta$, several optimizations were conducted and in Figure 6 the relation between the optimized mixer performance and the allowed pressure drop is shown. It is seen from the curve that the performance vs pressure drop relation is a monotonically decreasing function that approaches 0 for a large pressure drop. From the related design plots it can be seen that the topology is changing and is getting more entangled as the pressure drop is increased, yielding more complex mixing patterns.

A design with this complexity would be difficult if not impossible to obtain with traditional shape optimization techniques. The basic design principle is that 'propeller blades' are connected to the pipe wall to enhance mixing without violating the pressure drop constraint. If manufacturing



DOI: 10.1002/fld

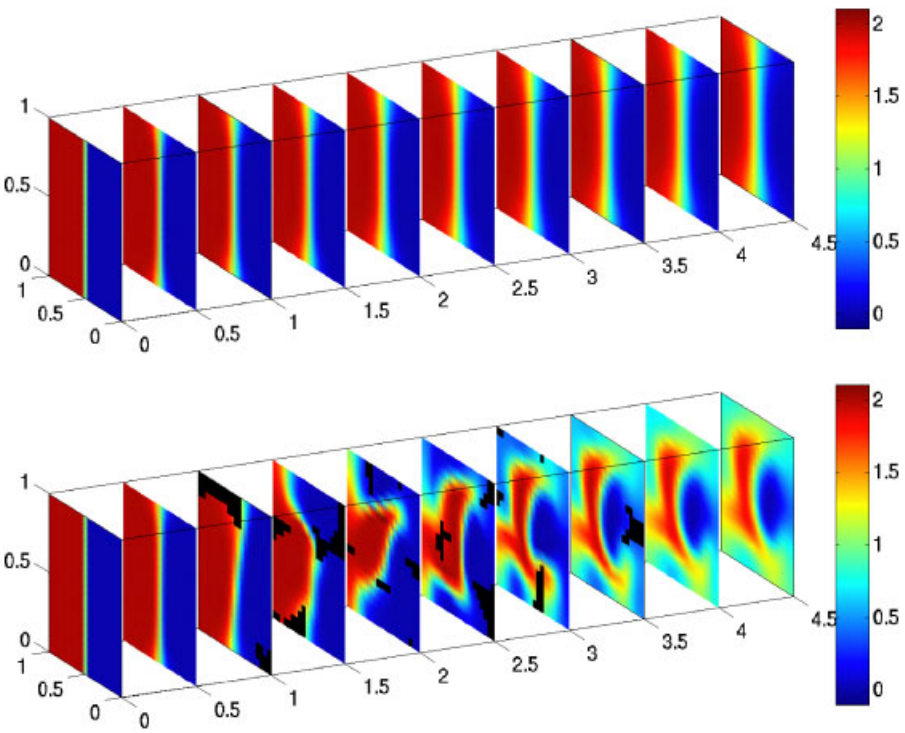


Figure 5. Concentration $\phi$ in several cross-sections showing the mixing progress of the unoptimized straight pipe mixer (upper) and the optimized mixer shown in Figure 4 (lower). Solid material ($\xi < 0.5$) in the cross-sections is colored black.

abilities prevent the realization of this complicated design, geometrical constraints like casting constraints could be added to the problem. In the following example, we ensure manufacturability by limiting the size of the design domain.

### *6.2. Micromixer with bottom layer design domain*

Many different micromixer designs have been presented in the literature having widely different performances [2, 36, 37]. This motivates the use of a general and systematic approach like topology optimization to optimize mixing performance. In order to do this a reference geometry, a section of a channel with the same dimensions as the staggered herringbone mixer by Stroock *et al*. [2], is introduced in Figure 7. The bottom part of the geometry is defined as the design domain. This subdomain consists of material with a low permeability, acting as a no-slip boundary. Letting the topology optimization procedure redistribute the material in the design domain, a new and optimized design appears as shown in Figure 8. As it is not possible for the optimizer to block the main fluid path the pressure constraint is no longer necessary and therefore deactivated. In Figure 8 the optimized topology for $Re = 0.01$ flow is shown. The topology includes well-known details from other micromixers. At the inlet 45° inclined grooves appear transitioning to herring bone-like structures at the center part of the channel and finally transforming back toward inclined grooves in the other direction. The performance of the optimized mixer is $\Phi_{\text{opt}} = 0.5594$ compared



DOI: 10.1002/fld

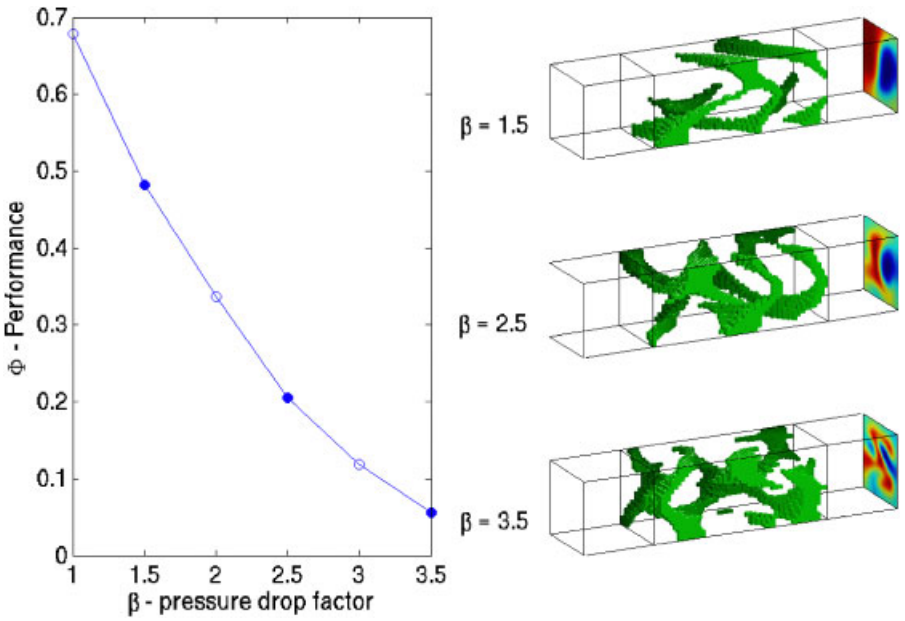


Figure 6. Variation of the allowed pressure drop factor $\beta$ for the straight pipe mixer. Left: performance vs pressure drop. Right: selected optimized mixers and the concentration distribution on the outlet face (Same coloring as in Figure 5, $\phi \in [0; 2]$).

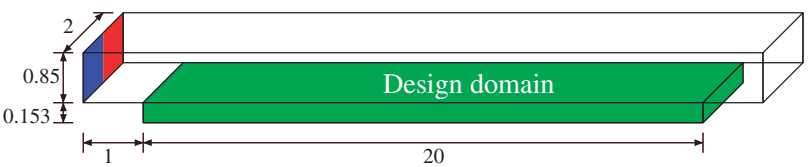


Figure 7. Problem figure showing the reference micromixer. The inlet velocity profile is parabolic in order to mimic fully developed laminar flow and the concentration profile is a Heaviside function. The total channel length is 22 ($\approx$12.9 times the hydraulic diameter) and the outlet is constructed similar to the inlet. The design domain is for the reference filled with material with a low permeability.

with the $\Phi_{\text{ref}} = 0.8114$ of the reference channel (see Figure 7), which is an improvement of 31% at the cost of 1.27 fold increase in pressure drop. The length of the modeled mixer is restricted due to limitations in computer time of our COMSOL implementation and therefore the mixer cannot be as long as those experimentally investigated in Stroock *et al*. [2]. Using the lowest $Re/Pe$ number from Stroock *et al*. [2], it is only possible to compute the performance of the mixer after one segment. Comparing the mixing performance it is seen that the reference performs better, but this is surely due to the limited resolution of the model. Many of those entanglements shown on the intensity pictures in the reference will definitely not be possible to resolve with the current COMSOL-based implementation.



DOI: 10.1002/fld

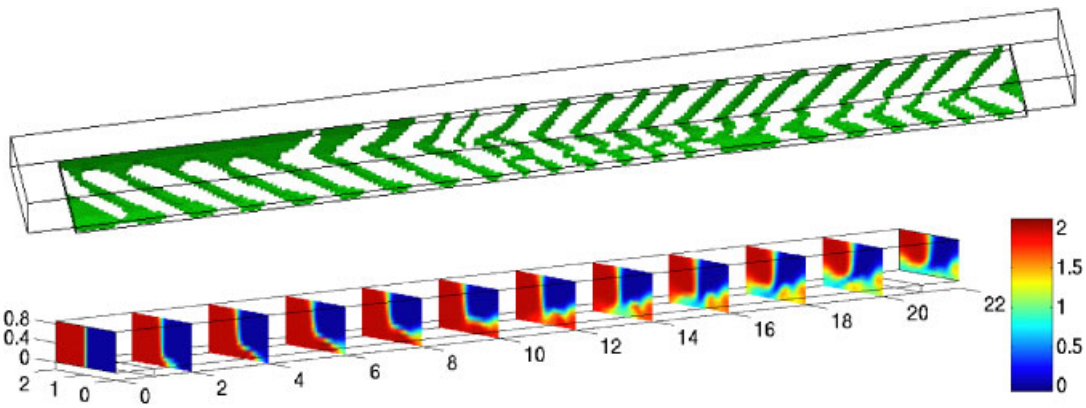


Figure 8. Optimized topology for the micromixer with bottom layer design domain having $Re = 0.01$, $Pe = 2000$. Top: design variables thresholded by $\xi < 0.5$ and colored by depth. Design variable distribution: $\xi < 0.1 : 20\%$, $\xi > 0.9 : 73\%$. Bottom: concentration $\phi$ plotted in several cross-sections along the mixer. Computed using $u1p1\phi1$ elements and by using 11520 design variables ($240 \times 24 \times 2$) in the bottom layer. Optimized performance $\Phi_{\text{final}} = 0.5594$, compared with $\Phi_{\text{ref}} = 0.8114$ improvement of 31% by the cost of a 1.27 fold increase in pressure drop. $\Delta p_{\text{final}} = 732.5$, $\Delta p_{\text{ref}} = 575.9$. Iterations: 641 with filter (radius = 0.1167) succeeded by 748 without filter. Total computation time was approx. 165 h.

Although this example suffers from a rough geometry description (known as the 'Duplo-syndrome' in the topology optimization community), it supports a combination of herringbones and slanted groves as optimal geometric shapes in micromixers, provided that manufacturing constraints only permit geometric variation in a bottom layer of the pipe cf. Figure 7. In addition, this study demonstrates that mixing performance is improved by varying the geometric pattern throughout the mixer. Hence, the topology optimization methodology goes beyond more traditional optimization studies using a parameter sweep on a fixed geometry, see e.g. Li and Chen [38] who also studied the mixer by Stroock *et al*. [2]. Also, it is concluded that periodically repeated mixers may be suboptimal.

## 7. DISCUSSION AND CONCLUSIONS

This study shows that topology optimization provides a systematic general approach for the design of microfluidic mixers. The first example presented shows that the method is capable of optimizing in-line mixers subjected to a constraint on the allowable pressure drop. The second example shows that design details such as staggered herring bones and slanted grooves appear when using this general and systematic approach. The designs are very similar to the ones experimentally investigated by Stroock *et al*. [2] exhibiting chaotic advection.

The examples considered have been run at Péclet numbers of $Pe = \{1000, 2000\}$ for low Reynolds number flows, hence, a gap remains in the experimental conditions reported in Stroock *et al*. [2]. From a computational point of view the larger the *Pe* number, the larger the domain needed in order to model say 50% mixing, which in turn increases the problem sizes beyond our computational capabilities with the present COMSOL implementation. Nevertheless, apart from verifying the



DOI: 10.1002/fld

approach, our simulations in the chosen parameter regime may help to improve the understanding of the basic design principles, which enhance micromixer performance.

To provide more practical results, the effect of imposing manufacturing constraints, such as symmetry in a cross-section of the pipe, would be a relevant direction of research as it would give the possibility of enhancing the geometric complexity while staying within the limits of available manufacturing technologies.

## ACKNOWLEDGEMENTS

The authors thank the TopOpt group (www.topopt.dtu.dk) at the Technical University of Denmark for fruitful discussions related to this paper.

## REFERENCES

1. Ottino JM, Wiggins S. Introduction: mixing in microfluidics. *Philosophical Transactions of the Royal Society A*: *Mathematical*, *Physical and Engineering Sciences* 2004; **362**(1818):923–935. DOI: 10.1098/rsta.2003.1355.
2. Stroock AD, Dertinger SKW, Ajdari A, Mezic I, Stone HA, Whitesides GM. Chaotic mixer for microchannels. *Science* 2002; **295**(5555):647–651. DOI: 10.1126/science.1066238.
3. Bendsøe MP, Kikuchi N. Generating topologies in structural design using a homogenization method. *Computer Methods in Applied Mechanics and Engineering* 1988; **71**:197–224. DOI: 10.1016/0045-7825(88)90086-2.
4. Bendsøe MP, Sigmund O. *Topology Optimization—Theory*, *Methods and Applications* (2nd edn). Springer: Berlin, 2003.
5. Pironneau O. On optimum profiles in Stokes flow. *Journal of Fluid Mechanics* 1973; **59**:117–128.
6. Borrvall T, Petersson J. Topology optimization of fluids in Stokes flow. *International Journal for Numerical Methods in Fluids* 2003; **41**(1):77–107. DOI: 10.1002/fld.426.
7. Evgrafov A. The limits of porous materials in the topology optimization of Stokes flows. *Applied Mathematics and Optimization* 2005; **52**(3):263–277. DOI: 10.1007/s00245-005-0828-z.
8. Guest JK, Prévost JH. Topology optimization of creeping fluid flows using a Darcy–Stokes finite element. *International Journal for Numerical Methods in Engineering* 2006; **66**(3):461–484. DOI: 10.1002/nme.1560.
9. Wiker N, Klarbring A, Borrvall T. Topology optimization of regions of Darcy and Stokes flow. *International Journal for Numerical Methods in Engineering* 2007; **69**(7):1374–1380. DOI: 10.1002/nme.1811.
10. Gersborg-Hansen A, Sigmund O, Haber R. Topology optimization of channel flow problems. *Structural and Multidisciplinary Optimization* 2005; **30**:181–192. DOI: 10.1007/s00158-004-0508-7.
11. Olesen LH, Okkels F, Bruus H. A high-level programming language implementation of topology optimization applied to steady-state Navier–Stokes flow. *International Journal for Numerical Methods in Engineering* 2006; **65**(7):975–1001. DOI: 10.1002/nme.1468.
12. Evgrafov A. Topology optimization of slightly compressible fluids. *ZAMM* 2006; **86**(1):46–62. DOI: 10.1002/zamm.200410223.
13. Thellner M. Multi-parameter topology optimization in continuum mechanics. *Ph.D. Thesis*, Department of Mechanical Engineering, Linköping University, 2005. ISBN-10 91-8529-71-2.
14. Gersborg-Hansen A. Topology optimization of flow problems. *Ph.D. Thesis*, Department of Mathematics and Department of Mechanical Engineering, Solid Mechanics, Technical University of Denmark, DCAMM Special Report S96, 2007. ISBN-10 87-90416-23-6.
15. Okkels F, Bruus H. Scaling behavior of optimally structured catalytic microfluidic reactors. *Physical Review E* 2007; **75**(1):016301. DOI: 10.1103/PhysRevE.75.016301.
16. Pingen G, Evgrafov A, Maute K. Topology optimization of flow domains using the lattice Boltzmann method. *Structural and Multidisciplinary Optimization* 2007; **34**(6):507–524. DOI: 10.1007/s00158-007-0105-7.
17. Evgrafov A, Pingen G, Maute K. Topology optimization of fluid domains: kinetic theory approach. *ZAMM* 2008; **88**(2):129–141. DOI: 10.1002/zamm.200700122.
18. Aage N, Poulsen TH, Gersborg-Hansen A, Sigmund O. Topology optimization of large scale Stokes flow problems. *Structural and Multidisciplinary Optimization* 2008; **35**:175–180. DOI: 10.1007/s00158-007-0128-0.

19. Guest JK, Prévost JH. Optimizing multifunctional materials: design of microstructures for maximized stiffness and fluid permeability. *International Journal of Solids and Structures* 2006; **43**:7028–7047. DOI: 10.1016/j.ijsolstr.2006.03.001.
20. Othmer C. A continuous adjoint formulation for the computation of topological and surface sensitivities of ducted flows. *International Journal for Numerical Methods in Fluids* 2008; Published on-line. DOI: 10.1002/fld.1770.
21. Brooks AN, Hughes TJR. Streamline upwind/Petrov–Galerkin formulations for convection dominated flows with particular emphasis on the incompressible Navier–Stokes equations. *Computer Methods in Applied Mechanics and Engineering* 1982; **32**(1–3):199–259. DOI: 10.1016/0045-7825(82)90071-8.
22. Hughes TJR, Franca LP. A new finite element formulation for computational fluid dynamics: VII. The Stokes problem with various well-posed boundary conditions: symmetric formulations that converge for all velocity/pressure spaces. *Computer Methods in Applied Mechanics and Engineering* 1987; **65**(1):85–96. DOI: 10.1016/0045-7825(87)90184-8.
23. Zienkiewicz OC, Taylor RL. *The Finite Element Method—Volume 3*: *Fluid Dynamics*. Butterworth Heinemann: London, 2000.
24. Donea J, Hureta A. *Finite Element Methods for Flow Problems*. Wiley: West Sussex, 2003.
25. Tezduyar TE, Ramakrishnan S, Sathe S. *International Journal for Numerical Methods in Fluids* 2008; Published on-line. DOI: 10.1002/fld.1743.
26. Masud A, Hughes TJR. A stabilized mixed finite element method for Darcy Flow. *Computer Methods in Applied Mechanics and Engineering* 2002; **191**:4341–4370. DOI: 10.1016/S0045-7825(02)00371-7.
27. Codina R. Comparison of some finite element methods for solving the diffusion–convection–reaction equation. *Computer Methods in Applied Mechanics and Engineering* 1998; **156**:185–210. DOI: 10.1016/S0045-7825(97)00206-5.
28. Svanberg K. The method of moving asymptotes—a new method for structural optimization. *International Journal for Numerical Methods in Engineering* 1987; **24**:359–373. DOI: 10.1002/nme.1620240207.
29. Vidal CA, Lee HS, Haber RB. The consistent tangent operator for design sensitivity analysis of history-dependent response. *Computing Systems Engineering* 1991; **2**:509–523.
30. Michaleris P, Tortorelli DA, Vidal CA. Tangent operators and design sensitivity formulations for transient non-linear coupled problems with applications to elastoplasticity. *International Journal for Numerical Methods in Engineering* 1994; **37**(14):2471–2499. DOI: 10.1002/nme.1620371408.
31. Choi K, Kim NH. *Structural Sensitivity Analysis and Optimization*. vols 1 and 2. Springer: Berlin, 2005. ISBN 03872-3336-9.
32. Sigmund O, Petersson J. Numerical instabilities in topology optimization: a survey on procedures dealing with checkerboards, mesh-dependencies and local minima. *Structural Optimization* 1998; **16**(1):68–75. DOI: 10.1007/BF01214002.
33. Bruns TE, Tortorelli DA. Topology optimization of non-linear elastic structures and compliant mechanisms. *Computer Methods in Applied Mechanics and Engineering* 2001; **190**(26–17):3443–3459. DOI: 10.1016/S0045-7825(00)00278-4.
34. Bourdin B. Filters in topology optimization. *International Journal for Numerical Methods in Engineering* 2001; **50**:2143–2158. DOI: 10.1002/nme.116.
35. Sigmund O. Morphology-based black and white filters for topology optimization. *Structural and Multidisciplinary Optimization* 2007; **33**:401–424. DOI: 10.1007/s00158-006-0087-x.
36. Liu RH, Stremler MA, Sharp KV, Olsen MG, Santiago JG, Adrian RJ, Aref H, Beebe DJ. Passive mixing in a three-dimensional serpentine microchannel. *Journal of Microelectromechanical Systems* 2000; **9**:190–197. DOI: 10.1109/84.846699.
37. Yang JT, Huang K, Tung KY, Hu IC, Lyu PC. A chaotic micromixer modulated by constructive vortex agitation. *Journal of Micromechanics and Microengineering* 2007; **17**:2084–2092. DOI: 10.1088/0960-1317/17/10/021.
38. Li C, Chen T. Simulation and optimization of chaotic micromixer using lattice Boltzmann method. *Sensors and Actuators B* 2005; **106**(2):871–877. DOI: 10.1016/j.snb.2004.09.006.